



# Quantifying sediment transport on desert piedmonts using $^{10}\text{Be}$ and $^{26}\text{Al}$

Kyle K. Nichols<sup>a,\*</sup>, Paul R. Bierman<sup>a</sup>, Roger LeB. Hooke<sup>b</sup>,  
Erik M. Clapp<sup>a</sup>, Marc Caffee<sup>c</sup>

<sup>a</sup>School of Natural Resources and Department of Geology, University of Vermont, Burlington, VT, 05405, USA

<sup>b</sup>Department of Geological Sciences and Institute for Quaternary Studies, University of Maine, Orono, ME, 04496, USA

<sup>c</sup>Center for Accelerator Mass Spectrometry, Lawrence Livermore National Laboratory, Livermore, CA, 94550, USA

Received 10 September 1999; received in revised form 17 July 2001; accepted 5 October 2001

## 10 Abstract

11 In situ produced  $^{10}\text{Be}$  and  $^{26}\text{Al}$ , measured in 40 sediment samples collected from the Iron and Granite Mountain piedmonts,  
12 eastern Mojave Desert, provide a unique view of piedmont modification processes and process rates over the  $10^3$  to  $10^5$  year time  
13 scale. Cosmogenic nuclide-based models suggest that the Iron and Granite Mountains generate 0.11–0.13 and 0.082–0.097  $\text{m}^3$   
14 of sediment per year per meter of range front, respectively. The sediment moves down the piedmont in an active transport layer  
15 (ATL), which is 20 to 30 cm thick (based on visual observations, measurements of depth to a buried B-horizon, cosmogenic  
16 nuclide data, and maximum ephemeral channel depths). Sediment in this layer is well-mixed vertically and horizontally on the  
17  $10^2$  years time scale, indicating that the small ephemeral channels which dominate the piedmont surface migrate quickly.  
18 Interpretive models of increasing nuclide activities at depth in two pits suggest steady sediment deposition on the piedmont (at  
19 rates between 17–21 and 38–45  $\text{m Ma}^{-1}$ ) until the late Pleistocene epoch, when a discontinuity to markedly lower nuclide  
20 activities in the isotopically well-mixed active transport layer suggests that deposition stopped, a significant change in piedmont  
21 behavior. Nuclide activities in 10 amalgamated surface samples, each collected along a different 4-km-long transect, increase  
22 steadily away from the mountain front. Thus, we infer that sediment is uniformly dosed by cosmic rays as it is transported down  
23 the Iron and Granite Mountain piedmonts. Interpretive models suggest that long-term average sediment speeds down the Iron  
24 and Granite Mountain piedmonts are a few decimeters to a meter per year. © 2002 Published by Elsevier Science B.V.

25  
26 *Keywords:* Arid region sediment transport; Climate change; Cosmogenic nuclide; Desert geomorphology; Pediment; Piedmont

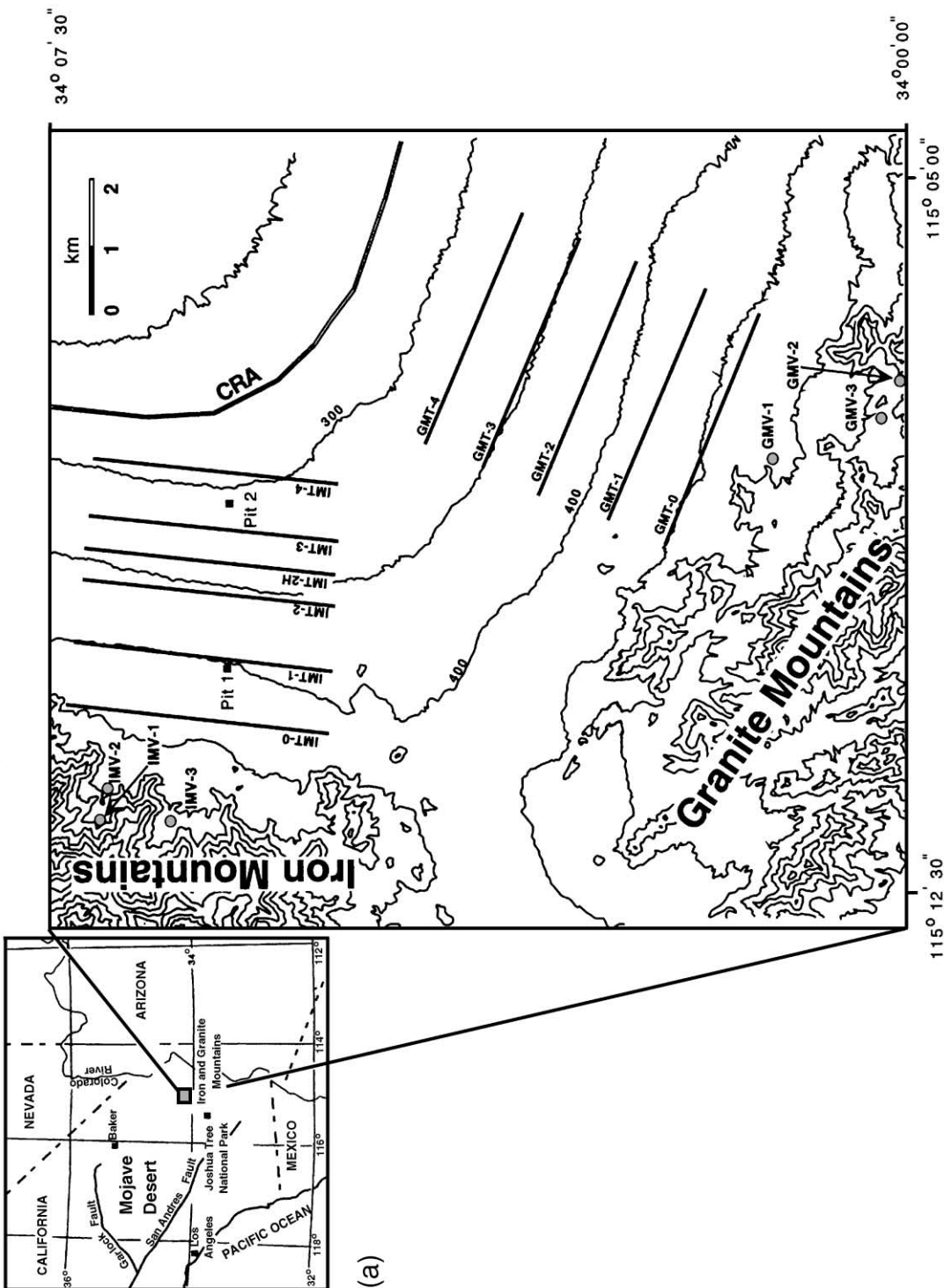
## 27 1. Introduction

28  
29  
30 Little is known about the rate and style of long-term  
31 sediment transport across desert piedmont surfaces  
32 (Denny, 1967; Hooke, 1968). Runoff is episodic in  
33 arid regions; thus, long-term observations, accom-

34 plished so far in only a few places worldwide, are ne- 34  
35 cessary to determine process rates. Rates determined 35  
36 over these human time scales may or may not be rep- 36  
37 resentative of rates on geologic time scales (Green- 37  
38 baum et al., 1999; Lekach and Schick, 1999; Yair, 38  
39 1999). Furthermore, the difficulty in determining accu- 39  
40 rate sediment generation rates in source basins has 40  
41 precluded quantitative estimates of sediment flux and 41  
42 sediment transport rates across piedmont surfaces. 42

\* Corresponding author.

E-mail address: kknichol@zoo.uvm.edu (K.K. Nichols).



(a)

(b)



Fig. 1. (a) Location of the Iron and Granite Mountains in the Mojave Desert, CA, and detailed contour map of the Iron and Granite Mountain piedmonts. On the contour map, straight black lines represent transect locations on the piedmont surfaces. IMT=Iron Mountain transect samples, GMT=Granite Mountain transect samples, IMT-2H=Iron Mountain transect where additional shallow pits were dug, but no sediment samples collected. Black squares represent soil pit locations. Gray circles represent valley sample locations. IMV=Iron Mountain valley samples and GMV=Granite Mountain valley samples. CRA=Colorado River Aqueduct. Contour interval is 50 m. Map based on the Granite Pass and East of Granite Pass U.S.G.S. 1:24,000 Quadrangles, 1985. (b) Oblique aerial photograph of the Iron and Granite Mountains and respective piedmonts looking to the southwest. Granite Mountains are on the left (south) and the Iron Mountains are on the right (west). Steep, narrow source basins for each piedmont penetrate mountains normal to rangefront. View is ~ 10 km wide.

43 Traditional geomorphic techniques of mapping,  
 44 monitoring, and observing soil development have elu-  
 45 cidated surface histories and piedmont ages. These are  
 46 useful for inferring changes in piedmont process (Bir-  
 47 keland, 1984; Wells et al. 1987; McFadden et al., 1989;  
 48 Bull, 1991), changes that are routinely attributed to  
 49 climatic fluctuations (Oberlander, 1974; Mayer and  
 50 Bull, 1981; Dohrenwend, 1987; Bull, 1991). For exam-  
 51 ple, Bull and Schick (1979) and Bull (1991) suggested  
 52 that soil was stripped off desert hillslopes and trans-  
 53 ported down gradient as a result of the change from a  
 54 wetter to a drier climate at the Pleistocene/Holocene  
 55 transition. Similarly, Wells et al. (1987) associated in-  
 56 creased drainage basin sediment yield with early Hol-  
 57 ocene deposition on piedmonts. They suggested that,  
 58 once the reservoir of sediment stored in mountain

basins was depleted, transport capacity of channels  
 increased and at least some piedmonts were dissected.

Previous studies of desert piedmonts have been  
 unable to address the long-term rate and distribution  
 of germane surface processes such as sediment trans-  
 port and deposition. By using a new tool, in situ  
 produced cosmogenic  $^{10}\text{Be}$  and  $^{26}\text{Al}$ , a novel sampling  
 strategy, and interpretive models, we quantify long-  
 term average sediment transport rates across large,  
 planar, piedmont surfaces that extend more than 10  
 km from the Iron and Granite Mountains in the Mojave  
 Desert, California (Fig. 1). Application of these tech-  
 niques elsewhere could lead to a better understanding  
 of arid-region sediment transport and surface pro-  
 cesses on desert piedmonts including the effects of  
 climate change.

59  
60  
61  
62  
63  
64  
65  
66  
67  
68  
69  
70  
71  
72  
73  
74

75 **2. Research area**

76 In the Mojave Desert, the Iron and Granite Moun-  
 77 tains rise steeply from adjacent, low-gradient ( $\sim 2^\circ$ )  
 78 piedmonts (Fig. 1). The piedmont surfaces consist  
 79 primarily of grus, 0.5 to 1 mm in diameter. There is  
 80 minimal carbonate development in the soils (Fig. 2).  
 81 Small ephemeral channels, averaging 10 cm in depth  
 82 (Nichols and Bierman, in press), migrate across the  
 83 planar piedmonts and account for the majority of  
 84 sediment transport (Bull, 1977). Almost all surface  
 85 clasts are unvarnished; desert pavements are not well  
 86 developed and there is no significant channel incision.  
 87 These and other field observations suggest that the  
 88 ephemeral channel network has relatively recently  
 89 reworked most ( $>98\%$ ) of the piedmont surface. The  
 90 remainder, directly abutting the range front, is relict  
 91 alluvium exhibiting some pavement development and  
 92 incision by channels 0.5 to 5 m deep. There is no  
 93 evidence for range-bounding faults, suggesting that the  
 94 basin and adjacent ranges are not currently tectonically  
 95 active.

96 The southern Mojave Desert and the Iron and  
 97 Granite Mountain piedmonts are extremely dry and  
 98 warm. Average annual precipitation is 79 mm and the  
 99 mean temperatures for January and July are 12 and 35  
 100  $^\circ\text{C}$ , respectively (NOAA, 1982). Packrat midden data  
 101 indicate a change in the climate from wetter to drier  
 102 conditions between 10,000 and 8000 years ago (Spaul-  
 103 ding et al., 1983; Spaulding and Graumlich, 1986).

104 **3. Cosmogenic nuclides**

105 Cosmic rays bombard Earth's surface and produce a  
 106 variety of nuclides in situ including  $^{10}\text{Be}$  and  $^{26}\text{Al}$ .  
 107 Cosmogenic nuclide production rates are greatest at  
 108 the surface and decrease exponentially with depth (Lal,  
 109 1988). For example, production rates at a depth of 1 m  
 110 in sediment ( $\rho = 1.55 \text{ g cm}^{-3}$ ) are 37% of surface  
 111 production. Production rates for  $^{10}\text{Be}$  and  $^{26}\text{Al}$ , and  
 112 the adjustments for altitude and latitude, have been  
 113 estimated, but remain uncertain at the 10% to 20%  
 114 level (Nishiizumi et al., 1989; Lal, 1991; Clark et al.,  
 115 1995; Bierman et al., 1996; Dunai, 2000; Desilets and  
 116 Zereda, 2000). We can measure  $^{10}\text{Be}$  and  $^{26}\text{Al}$  activ-  
 117 ities (to  $\pm 4\%$  precision or better) using accelerator  
 118 mass spectrometry. We use these nuclides as cosmic-

ray dosimeters to record near-surface residence time. 119  
 Using quantitative and qualitative geomorphic models, 120  
 we interpret measured  $^{10}\text{Be}$  and  $^{26}\text{Al}$  activities in terms 121  
 of integrated cosmic-ray dosing. From this informa- 122  
 tion, we estimate sediment transport rates expressed as 123  
 average grain speeds down piedmont. 124

**4. Methods** 1254.1. *Sediment collection for  $^{10}\text{Be}$  and  $^{26}\text{Al}$  analysis* 126

To understand and quantify the three-dimensional 128  
 behavior of the Iron and Granite Mountains and their 129  
 piedmonts over time, we collected three types of 130  
 samples: source valley alluvial sediment, piedmont 131  
 surface sediment, and sediment exposed in soil pits. 132  
 Measurement of  $^{10}\text{Be}$  and  $^{26}\text{Al}$  in sediment samples 133  
 collected from valleys at the Iron and Granite Moun- 134  
 tain range fronts allows quantification of long-term 135  
 average source-basin lowering rates and the flux of 136  
 sediment entering the piedmont (e.g., Brown et al., 137  
 1995; Bierman and Steig, 1996; Granger et al., 1996). 138  
 Integrated piedmont transect samples located at suc- 139  
 cessive 1-km intervals from the range front reflect 140  
 changes in average  $^{10}\text{Be}$  and  $^{26}\text{Al}$  activity as sediment 141  
 moves away from the source basins and allow us to 142  
 determine average sediment speed down piedmont. 143  
 Profiles of piedmont sediment exposed in soil pits 144  
 allow us to quantify the depth to which sediment is 145  
 currently well mixed and provide insight into whether 146  
 the piedmont is, or has been, a surface of deposition, 147  
 erosion, or transport. 148

4.1.1. *Source valley alluvial sediment samples* 149

We determined long-term basin erosion and sedi- 150  
 ment generation rates by analyzing fluvial sediment 151  
 samples collected from source valley alluvial channels 152  
 draining small, steep, lithologically homogeneous 153  
 basins in the Iron Mountains ( $n = 3$ ), and the Granite 154  
 Mountains ( $n = 2$ ) (Fig. 1). Each of these samples repre- 155  
 sents the integration of sediment transported out of 156  
 many small sub-basins and mixed by fluvial processes. 157  
 158

4.1.2. *Transect samples of piedmont sediment* 159

Five transects were laid out on the Iron and Granite 160  
 Mountain piedmonts. The transects were parallel to the 161  
 range fronts and were spaced at 1-km intervals down 162  
 163

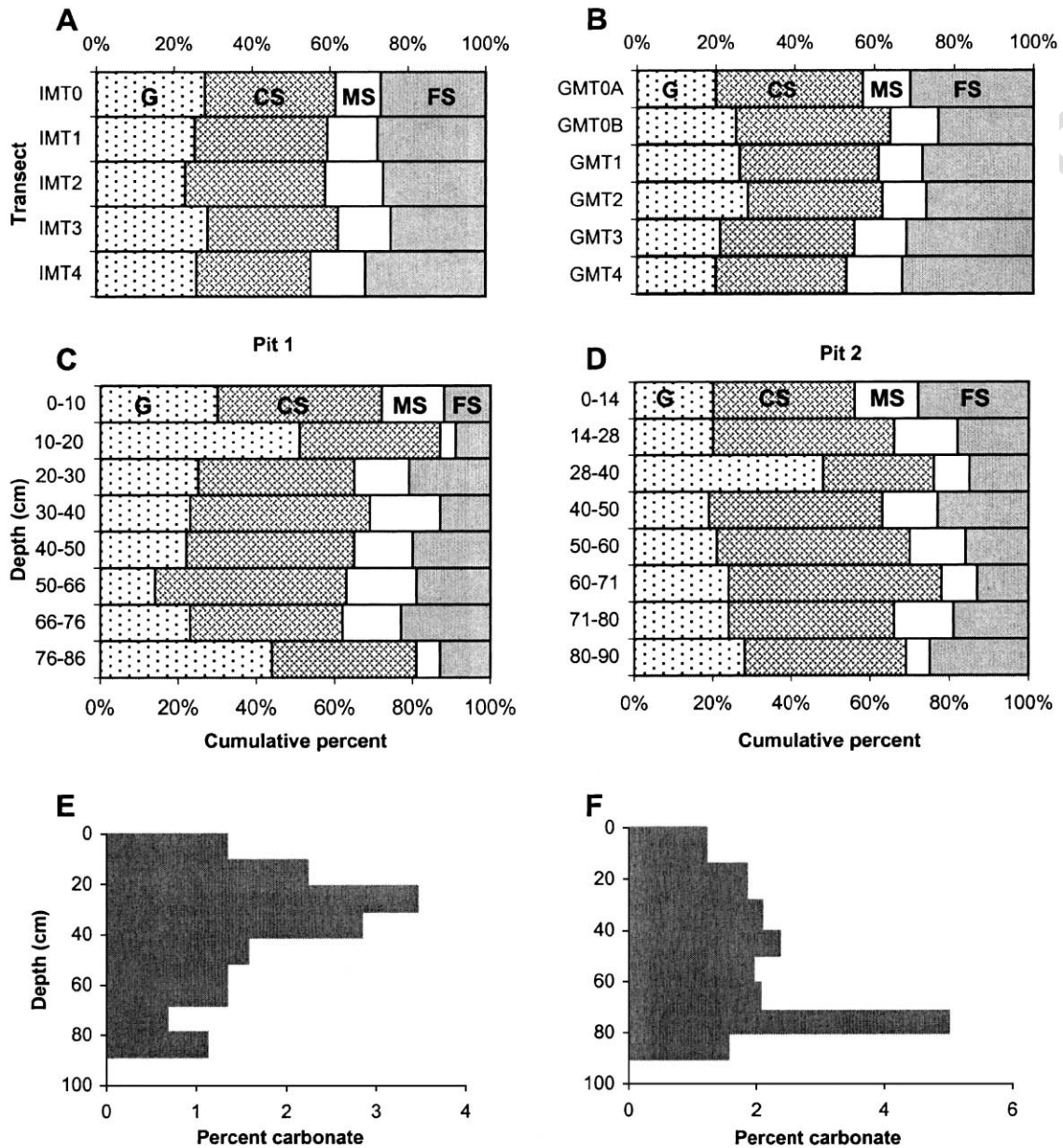


Fig. 2. Grain size and carbonate distribution of sediment collected from Iron and Granite Mountain piedmonts. G=gravel and larger, CS=coarse sand, MS=medium sand, and FS=fine sand and smaller. (A) Amalgamated Iron Mountain transect samples. No clear down-piedmont fining trend is observed. (B) Amalgamated Granite Mountain transect samples. No clear down-piedmont fining trend is observed. (C) Soil Pit 1. Grain size is uniform except for a gravel layers at depths of 10 to 20 cm and 76 to 86 cm. (D) Soil pit 2. Grain size is uniform except for gravel layer at depth of 28 to 40 cm. (E) Soil pit 1 carbonate percentage in less than 80  $\mu$ m fraction. Highest percentage is from 20 to 30 cm. (F) Soil pit 2 carbonate percentage. Highest percentage is from 71 to 80 cm.

164 the piedmont, starting at the respective range fronts.  
 165 Along each transect, we collected equal volumes of  
 166 surface sediment (0 to 10 cm deep) from 20 sampling  
 167 stations and amalgamated these 20 samples. The trans-  
 168 ects were 4 km long and the sampling stations were  
 169 spaced approximately 200 m apart (Fig. 1). The actual  
 170 locations of predetermined sampling stations were  
 171 established in the field using a hand-held Garmin 12  
 172 Global Positioning System (GPS); the horizontal  
 173 uncertainty of uncorrected GPS measurements effec-  
 174 tively randomized ( $\pm 20$  m) actual sample locations  
 175 along the transects.

176 The piedmont consists of three distinct, low-relief  
 177 geomorphic units: low terraces 10 to 20 cm high),  
 178 active channels, and animal burrow piles (Fig. 3). We  
 179 classified each transect sampling station according to  
 180 the geomorphic unit that was sampled (Table 1). To  
 181 determine if low-terrace sediment has been exposed  
 182 on average longer than channel sediment and, thus, is  
 183 more heavily dosed by cosmic radiation, we collected  
 184 separate subsamples on two transects of both geo-  
 185 morphic units and compared the nuclide activities. We  
 186 also subsampled sediment from animal burrow piles  
 187 to determine the depth from which sediment was  
 188 transported vertically by burrowing. At each of the  
 189 20 sampling stations along transects IMT-1 and IMT-

190 4, we collected equal volumes of sediment from the  
 191 nearest terrace, channel, and animal burrow pile, and  
 192 amalgamated each type of sample separately.

193 A distinctive, rougher fan surface appeared to  
 194 extend into the northern four sampling stations along  
 195 IMT-0 (Fig. 1). Channels were entrenched and the  
 196 surface had a poorly developed pavement. To deter-  
 197 mine whether or not the difference in appearance was  
 198 reflected in nuclide activity, we collected a separate  
 199 subsample of sediment from only the four sampling  
 200 stations on the alluvial fan surface and amalgamated  
 201 these samples (IMT-0FAN). The IMT-0 transect sam-  
 202 ple contained sediment from all 20 sampling stations  
 203 (Table 1).  
 204

#### 4.1.3. Soil pit sediment samples

205  
 206 In the two soil pits on the Iron Mountain piedmont  
 207 (Fig. 1), we noted soil stratigraphy, sediment grain  
 208 size, and soil horizonation to a depth of about 1 m. On  
 209 the basis of soil stratigraphy, we divided each pit into  
 210 eight depth intervals that we sampled to determine  
 211 nuclide activity. Each interval was continuous so that  
 212 the entire soil profile was represented. We dug 25  
 213 additional shallow soil pits along IMT-1, IMT-2H, and  
 214 IMT-4 to understand better the spatial variability of  
 215 depth to the buried B-horizon.



Fig. 3. Photograph of ephemeral channels and terraces located near IMT-3. Unvegetated channel bottom contains the most recently transported sediment. Low terraces have sparse vegetation. There is no desert pavement. The channel in the middle of photograph is  $\sim 2$  m wide. Photograph taken looking southwest with the Iron Mountains in the right background.

t1.1 Table 1

t1.2 Distribution of geomorphic unit sampling stations along transect

t1.3 Sample <sup>a</sup>	Terrace	Channel bottom	Channel bank	Road	Animal burrow	Alluvial fan	Total of subsamples
t1.4 IMT-0	11	5	0	0	0	4	20
t1.5 IMT-0 FAN	0	0	0	0	0	4	4
t1.6 IMT-1	13	4	1	0	0	2	20
t1.7 IMT-1 CHAN	0	20	0	0	0	0	20
t1.8 IMT-1 TERR	20	0	0	0	0	0	20
t1.9 IMT-1 CRIT	0	0	0	0	20	0	20
t1.10 IMT-2	13	6	0	1	0	0	20
t1.11 IMT-3	9	10	0	1	0	0	20
t1.12 IMT-4	15	5	0	0	0	0	20
t1.13 IMT-4 CHAN	0	20	0	0	0	0	20
t1.14 IMT-4 TERR	20	0	0	0	0	0	20
t1.15 IMT-4 CRIT	0	0	0	0	20	0	20
t1.16 GMT-0A	13	5	2	0	0	0	20
t1.17 GMT-0B	10	7	1	1	1	0	20
t1.18 GMT-1	12	8	0	0	0	0	20
t1.19 GMT-2	12	8	0	0	0	0	20
t1.20 GMT-3	11	6	2	1	0	0	20
t1.21 GMT-4	11	6	2	1	0	0	20

<sup>a</sup> GMT = Granite Mountain transect samples, IMT = Iron Mountain transect samples, IMT-0 FAN = sediment from higher alluvial surface, IMT-#CHAN = Iron Mountain channel sediment, IMT-#TERR = Iron Mountain low terrace sediment, IMT-#CRIT = Iron Mountain animal burrow sediment GMT-0A and GMT-0B are field replicates sampled independently.

t1.22

216

## 217 4.2. Laboratory methods

218 All samples were sieved and weighed. We analyzed  
 219 the 0.5 to 1.0 mm size fraction to minimize inclusion of  
 220 aeolian input from other basins. We did not analyze  
 221 different grain sizes because ephemeral channels, such  
 222 as those on the Iron and Granite Mountain piedmonts,  
 223 are not armored and apparently do not preferentially  
 224 transport smaller grain sizes (Laronne and Reid, 1993;  
 225 Laronne et al., 1994; Reid and Laronne, 1995). This  
 226 conclusion is supported by previous research in arid-  
 227 region streams that suggests that all grain sizes have  
 228 statistically similar <sup>10</sup>Be and <sup>26</sup>Al activities (Clapp et  
 229 al., 2000; Clapp et al., 2001). Thus, we assume that  
 230 nuclide activities in the 0.5 to 1.0 mm size fraction that  
 231 we analyzed are representative of all fluvially transport-  
 232 ed material.

233 We measured the density and carbonate content of  
 234 all soil pit depth intervals. To measure the density, we  
 235 extracted a known volume of sediment from each  
 236 layer and weighed each sample. The density did not  
 237 vary systematically with depth and the average den-  
 238 sity of all strata was  $1.55 \pm 0.07 \text{ g cm}^{-3}$ . We used the  
 239 Chittick apparatus to measure carbonate content  
 240 (Machette, 1986). Based on the results of the carbo-  
 241 nate measurements (Fig. 2) and our soil pit observa-

tions, we classified the carbonate development as  
 Stage I.

Samples for nuclide analysis (0.5 to 1 mm) were  
 ultrasonically etched, once in heated 6 N HCl and up  
 to four times in heated 1% HF and 1% HNO<sub>3</sub> in  
 order to remove any atmospheric <sup>10</sup>Be and to isolate  
 at least 40 g of pure quartz (Kohl and Nishiizumi,  
 1992). After the addition of 250 μg of Be carrier, we  
 digested the samples with HF. Be and Al were puri-  
 fied using chromatographic techniques. The <sup>10</sup>Be/<sup>9</sup>Be  
 and <sup>26</sup>Al/<sup>27</sup>Al ratios were determined using acceler-  
 ator mass spectrometry (AMS) at Lawrence Liver-  
 more National Laboratory. All measurements were  
 corrected using similar-sized procedural blanks. Blanks  
 were prepared with each batch of seven samples and  
 analyzed at the same time as the other seven samples.  
 We calculated <sup>10</sup>Be and <sup>26</sup>Al activity from <sup>9</sup>Be (ad-  
 ded as carrier) and native <sup>27</sup>Al measured by Induc-  
 tively Coupled Argon Plasma Spectrometry–Optical  
 Emission in duplicate aliquots removed from HF so-  
 lutions.

## 4.3. Reproducibility

The nuclide data are reproducible. Field replication,  
 laboratory replication (Table 2), and the <sup>26</sup>Al/<sup>10</sup>Be

242

243

244

245

246

247

248

249

250

251

252

253

254

255

256

257

258

259

260

261

262

263

264

265

266

t2.1 Table 2

t2.2  $^{10}\text{Be}$  and  $^{26}\text{Al}$  data for the Iron and Granite Mountain piedmonts

Sample <sup>a</sup>	Elevation (m) <sup>b</sup>	Northing <sup>c,d</sup>	Easting <sup>c,d</sup>	Measured nuclide concentration (10 <sup>6</sup> atoms g <sup>-1</sup> ) <sup>e</sup>		Ratio $^{26}\text{Al}/^{10}\text{Be}$	Description
				$^{10}\text{Be}$	$^{26}\text{Al}$		
GMV-1	485	3766547	671919	0.168 ± 0.009	1.02 ± 0.06	6.08 ± 0.48	integrated valley sediment
GMV-2	600	3764501	672404	0.131 ± 0.005	0.82 ± 0.04	6.22 ± 0.40	integrated valley sediment
GMV-3	550	3765000	672274	0.148 ± 0.005	0.98 ± 0.05	6.65 ± 0.41	integrated valley sediment
GMT-0A	450	3767980,	670920,	0.188 ± 0.009	1.15 ± 0.06	6.10 ± 0.46	integrated transect sediment (20 sites)
GMT-0B		3766620	674540	0.191 ± 0.010	1.06 ± 0.10	5.58 ± 0.59	field replicate of GMT-0A
GMT-1	415	3768900,	671270,	0.213 ± 0.015	1.11 ± 0.16	5.21 ± 0.86	integrated transect sediment (20 sites)
GMT-2	380	3767530	674920	0.243 ± 0.010	1.57 ± 0.08	6.46 ± 0.42	integrated transect sediment (20 sites)
GMT-3	350	3769820,	671640,	0.290 ± 0.011	1.66 ± 0.10	5.71 ± 0.41	integrated transect sediment (20 sites)
GMT-4	320	3768440	675260	0.290 ± 0.011	1.66 ± 0.10	5.71 ± 0.41	integrated transect sediment (20 sites)
IMV-1	530	3770760,	672000,	0.316 ± 0.012	1.95 ± 0.10	6.18 ± 0.39	integrated transect sediment (20 sites)
IMV-2	495	3769400	675620	0.140 ± 0.004	0.91 ± 0.06	6.46 ± 0.46	integrated valley sediment
IMV-3	510	3771680,	672360,	0.162 ± 0.005	1.13 ± 0.07	6.93 ± 0.47	integrated valley sediment
IMT-0	425	3770320	675970	0.143 ± 0.004	0.99 ± 0.06	6.89 ± 0.45	integrated valley sediment
IMT-0FAN	440	3776603	666643	0.226 ± 0.010	1.38 ± 0.08	6.14 ± 0.45	integrated transect sediment (20 sites)
IMT-1	400	3777034,	668460,	0.212 ± 0.008	1.37 ± 0.11	6.46 ± 0.57	integrated alluvial fan sediment (4 sites)
IMT-1CHAN		3773103	668011	0.245 ± 0.008	1.46 ± 0.07	5.98 ± 0.36	integrated transect sediment (20 sites)
IMT-1CRIT		3777034,	668460,	0.252 ± 0.011	1.51 ± 0.08	6.00 ± 0.42	integrated channel sediment (20 sites)
IMT-1TERR		3776442	668402	0.259 ± 0.008	1.68 ± 0.09	6.51 ± 0.40	integrated animal burrow sediment (20 sites)
IMT-2	355	3776958,	669428,	0.258 ± 0.011	1.53 ± 0.10	5.95 ± 0.46	integrated terrace sediment (20 sites)
IMT-3	320	3773033	669010	0.286 ± 0.009	1.87 ± 0.11	6.54 ± 0.43	integrated transect sediment (20 sites)
IMT-4	290	3772997	669974	0.320 ± 0.013	2.04 ± 0.12	6.37 ± 0.46	integrated transect sediment (20 sites)
IMT-3DUP		3776850,	671359,	0.325 ± 0.010	1.90 ± 0.10	5.86 ± 0.35	laboratory replicate of IMT-3
IMT-4CHAN		3772898	670988	0.367 ± 0.100	2.38 ± 0.12	6.49 ± 0.36	integrated transect sediment (20 sites)
IMT-4CRIT		3772847	671975	0.393 ± 0.019	2.16 ± 0.13	5.49 ± 0.42	integrated channel sediment (20 sites)
IMT-4CRIT				0.392 ± 0.019	2.24 ± 0.12	5.71 ± 0.41	integrated animal burrow sediment (20 sites)

Table 2 (continued)

Sample <sup>a</sup>	Elevation (m) <sup>b</sup>	Northing <sup>c,d</sup>	Easting <sup>c,d</sup>	Measured nuclide concentration (10 <sup>6</sup> atoms g <sup>-1</sup> ) <sup>e</sup>		Ratio <sup>26</sup> Al/ <sup>10</sup> Be	Description
				<sup>10</sup> Be	<sup>26</sup> Al		
t2.29							
t2.30							
IMT-4TERR				0.380 ± 0.020	2.24 ± 0.12	5.89 ± 0.43	integrated terrace sediment (20 sites)
t2.31							
PIT1 0-10	405	3774990	679030	0.194 ± 0.015	1.10 ± 0.08	5.67 ± 0.57	integrated soil pit sediment
t2.32							
PIT1 10-20				0.193 ± 0.007	1.21 ± 0.08	6.29 ± 0.45	integrated soil pit sediment
t2.33							
PIT1 20-30				0.299 ± 0.014	1.73 ± 0.11	5.80 ± 0.44	integrated soil pit sediment
t2.34							
PIT1 30-40				0.328 ± 0.011	2.01 ± 0.10	6.12 ± 0.38	integrated soil pit sediment
t2.35							
PIT1 40-50				0.352 ± 0.011	2.09 ± 0.11	5.94 ± 0.36	integrated soil pit sediment
t2.36							
PIT1 50-66				0.385 ± 0.013	2.51 ± 0.13	6.52 ± 0.40	integrated soil pit sediment
t2.37							
PIT1 66-76				0.403 ± 0.020	2.44 ± 0.14	6.06 ± 0.45	integrated soil pit sediment
t2.38							
PIT1 76-86				0.427 ± 0.026	2.51 ± 0.13	5.89 ± 0.47	integrated soil pit sediment
t2.39							
PIT2 0-14	310	3774990	671500	0.404 ± 0.012	2.54 ± 0.13	6.29 ± 0.38	integrated soil pit sediment
t2.40							
PIT2 0-14DUP				0.441 ± 0.013	2.38 ± 0.12	5.38 ± 0.32	laboratory replicate of PIT2 0-14
t2.41							
PIT2 14-28				0.411 ± 0.016	2.65 ± 0.15	6.44 ± 0.44	integrated soil pit sediment
t2.42							
PIT2 28-40				0.468 ± 0.015	2.74 ± 0.14	5.86 ± 0.36	integrated soil pit sediment
t2.43							
PIT2 40-50				0.473 ± 0.015	2.99 ± 0.15	6.33 ± 0.38	integrated soil pit sediment
t2.44							
PIT2 50-60				0.479 ± 0.016	2.91 ± 0.16	6.08 ± 0.40	integrated soil pit sediment
t2.45							
PIT2 60-71				0.477 ± 0.014	2.84 ± 0.16	5.95 ± 0.37	integrated soil pit sediment
t2.46							
PIT2 71-80				0.496 ± 0.015	3.00 ± 0.15	6.05 ± 0.34	integrated soil pit sediment
t2.47							
PIT2 80-90				0.513 ± 0.015	3.00 ± 0.15	5.84 ± 0.33	integrated soil pit sediment
t2.48							

<sup>a</sup> GMV=Granite Mountain valley samples, GMT=Granite Mountain transect samples, IMV=Iron Mountain valley samples IMT=Iron Mountain transect samples, IMT-0FAN=sediment from higher alluvial surface, IMT-#CHAN=Iron Mountain channel channel sediment, IMT-#CRIT=Iron Mountain animal burrow sediment, IMT-#TERR=Iron Mountain low terrace sediment, PIT1=soil pit 1 sediment, PIT2=soil pit 2 sediment, DUP=laboratory replicate.

<sup>b</sup> Measured from Granite Pass and East of Granite Pass U.S.G.S. quadrangles, 1985, average elevation for transect samples.

<sup>c</sup> Measured using Garmin 12 GPS, UTM zone 11S, NAD 27 coordinate system.

<sup>d</sup> Transect samples are denoted by the two endpoint coordinates.

<sup>e</sup> Error is counting statistics of AMS, with 2% uncertainty for stable Be and 4% uncertainty for stable Al combined quadratically.

267 regression validate the method of collecting integrated  
268 samples and the laboratory procedures. Measured  
269 yields of Be carrier average  $100.6 \pm 1.1\%$ ; measured  
270 yields of Al blanks average  $99.7 \pm 0.9\%$ , indicating  
271 high recovery of stable Al. Nuclide activities of GMT-

0A and B, collected independently along the same  
transect, are statistically indistinguishable for both <sup>26</sup>Al  
and <sup>10</sup>Be activity (Fig. 4). IMT-3 was analyzed twice;  
both analyses produced statistically similar results for  
both <sup>26</sup>Al and <sup>10</sup>Be (Fig. 4). Considering the entire data

272  
273  
274  
275  
276

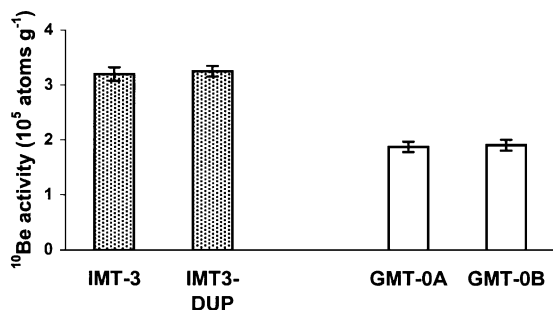


Fig. 4. Reproducibility of sediment samples. GMT-0A and GMT-0B were collected independently. IMT-3 and IMT-3DUP are laboratory replicates. Error bars represent  $1\sigma$  analytical error.

set,  $^{10}\text{Be}$  and  $^{26}\text{Al}$  are well correlated with a ratio of  $5.8 \pm 0.2$  and an intercept of  $0.07 \pm 0.5 \times 10^5$  atoms at a 68% confidence level (Fig. 5). Since the  $^{26}\text{Al}$  data mirror the  $^{10}\text{Be}$  data, we focus discussion, for the most part, on the  $^{10}\text{Be}$  data. None of our samples have  $^{26}\text{Al}/^{10}\text{Be}$  ratios low enough to suggest significant burial on the  $10^5$  years time scale.

284 **5. Results**

285 Three independent data sets help us understand  
 286 sediment transport processes and estimate rates of  
 287 landscape change on the Iron and Granite Mountain  
 288 piedmonts. Integrated transect nuclide data allow  
 289 estimation of sediment transport rates down the pied-  
 290 monts. Soil development, soil pit nuclide data, and  
 291 ephemeral channel depths in two soil pits reflect the

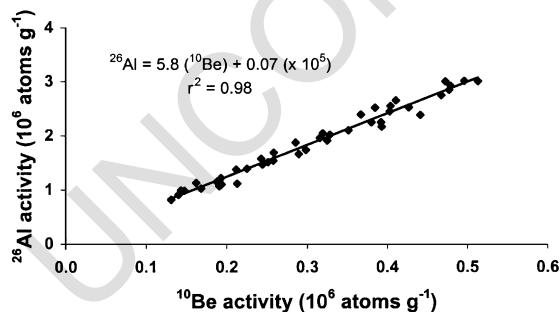


Fig. 5.  $^{10}\text{Be}$  and  $^{26}\text{Al}$  data are well correlated ( $r^2 = 0.98$ ). Slope of  $5.8 \pm 0.2$  (68% confidence level) is consistent with production ratio of 6.0 (Nishiizumi et al., 1989) and suggests that sediment samples were not buried for significant periods of time ( $>10^5$  years).

depth to which piedmont sediment is well-mixed and, thus, surface histories at these two specific sites. Nuclide activity in source valley alluvial sediment samples allows us to quantify the sediment flux to the piedmonts from mountain drainage basins. Together, these data provide a four-dimensional (including time) view of sediment movement into and across the Iron and Granite Mountain piedmonts on a  $10^4$  to  $10^5$  years time scale.

5.1. Piedmont sediment transect data

Integrated transect samples show a remarkably regular increase in nuclide activity down gradient, the rate of which is statistically indistinguishable between the two piedmonts (Fig. 6). The similarity of the transect sample regression slopes suggests that cosmic ray dosing rates, as a function of distance down both piedmonts, are similar. In addition, the nuclide activity ( $^{10}\text{Be}$  and  $^{26}\text{Al}$ ) in terrace, channel, and burrow

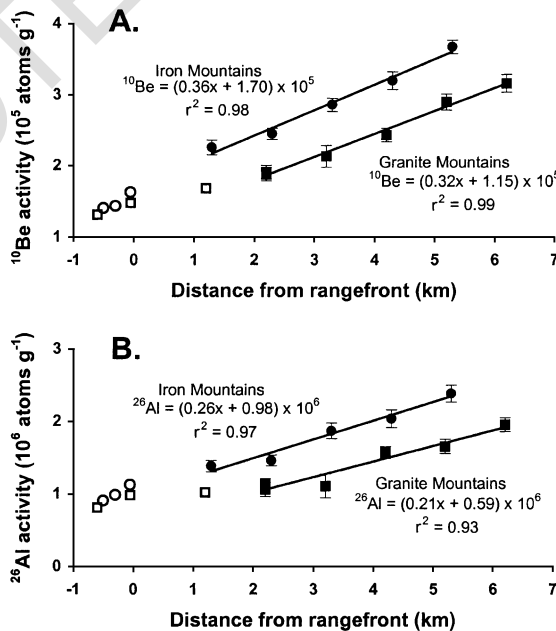


Fig. 6. Transect (closed symbols) and valley (open symbols) data from Iron (circles) and Granite (squares) Mountain piedmonts. (A)  $^{10}\text{Be}$  transect data. (B)  $^{26}\text{Al}$  transect data. Slopes for nuclide activity as a function of distance from range front are indistinguishable at the 68% confidence level. Error bars represent  $1\sigma$  analytical error. Error bars for valley samples are same size as symbols.

311 pile sediment is indistinguishable across gradient (Fig.  
 312 7). Similar nuclide activities between channel and  
 313 terrace sediment imply that channels migrate across  
 314 the surface on a time-scale comparable to or less than  
 315 the average cosmogenic nuclide detection limit (the  
 316 time required to produce the number of atoms that the  
 317 AMS could count outside the  $1\sigma$  error, or about 1000  
 318 years at our sites). The similarity between nuclide  
 319 activity in animal burrow sediment and that in terrace  
 320 and channel sediment suggests that sediment is well  
 321 mixed to the depth that most animals burrow, presu-  
 322 mably less than or equal to the depth of ephemeral  
 323 channel incision. Sediment on the alluvial fan surface  
 324 (IMT-0FAN) is no more highly dosed than sediment on  
 325 the adjacent active piedmont surface (Tables 1 and 2),  
 326 implying that sediment exposure histories on a  $10^3$   
 327 years time scale are similar along IMT-0, regardless of  
 328 surface topography.

329  
 330 5.2. Soil pit data

331 Four lines of evidence suggest that the upper 20 to  
 332 30 cm of sediment on the Iron Mountain piedmont, and  
 333 by inference the Granite Mountain piedmont, are  
 334 vertically well mixed and distinct from underlying  
 335 material. (1) The top two samples from both soil pits  
 336 have statistically indistinguishable  $^{10}\text{Be}$  activity (Fig.  
 337 8). (2) A sharp contact between overlying gray bedded  
 338 sediment and underlying red massive sediment (also  
 339 noted in 25 additional shallow pits along transects  
 340 IMT-1, IMT-2H, and IMT-4), occurs on average 20 to

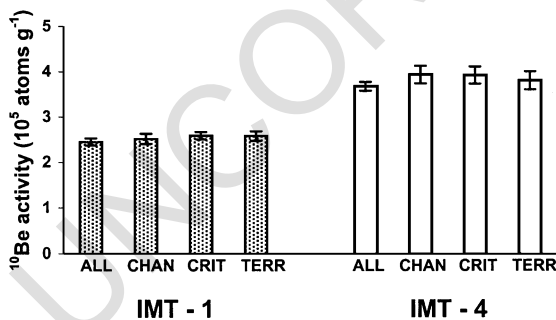


Fig. 7. Different geomorphic units along the same transect have similar nuclide activities. ALL=amalgamated sediment, CHAN=channel sediment, TERR=terrace sediment, and CRIT=animal burrow sediment exposed at surface. Error bars represent  $1\sigma$  analytical error.

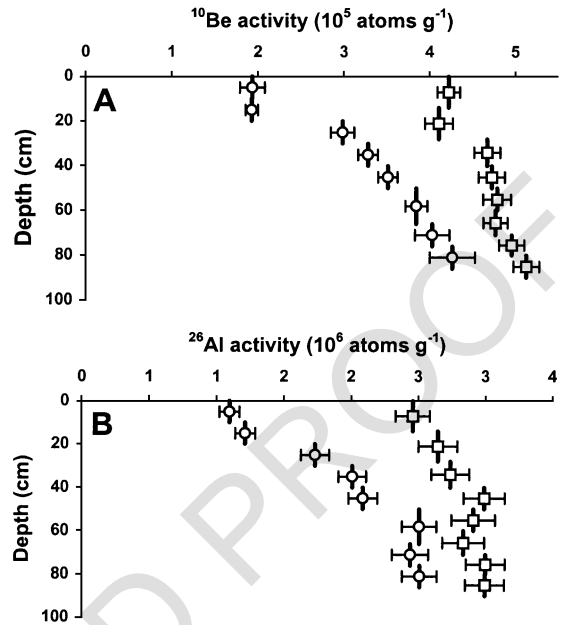


Fig. 8. Data from soil pit samples showing increasing nuclide activities at depth. Pit 1 (circles) is about 2.2 km from the Iron Mountain rangefront and pit 2 (squares) is about 4.7 km from the Iron Mountain rangefront. (A)  $^{10}\text{Be}$  soil pit data. (B)  $^{26}\text{Al}$  soil pit data. Horizontal bars represent  $1\sigma$  analytical uncertainty. Vertical bars represent thickness of integrated sample.

341 30 cm below the surface. The underlying reddened  
 342 material is a buried B-horizon ( $B_b$ ), the color of which  
 343 suggests at least several thousand years of stability  
 344 (Birkeland, 1984). (3) Over 9000 topographic mea-  
 345 surements of the ephemeral channels, currently the  
 346 primary means by which sediment is mixed and trans-  
 347 ported, show maximum channel depths between 20  
 348 and 30 cm, comparable to the depth of bedded sedi-  
 349 ment overlying the  $B_b$ -horizon (Nichols and Bierman,  
 350 in press). (4) Transect samples taken from terraces,  
 351 channels, and animal burrow piles have statistically  
 352 similar nuclide activities, implying thorough mixing of  
 353 the uppermost 20 to 30 cm of piedmont sediment on  
 354 the  $10^2$  years time scale (Fig. 7).

355 For the remainder of the paper, we refer to the well-  
 356 mixed layer, the upper  $25 \pm 5$  cm of piedmont soil as  
 357 the active transport layer (ATL) (Lekach et al., 1998).  
 358 We believe that sediment in the ATL is episodically in  
 359 transport down piedmont because this layer is the  
 360 same thickness as the maximum channel depths, dis-  
 361 plays sedimentary structures, and lacks soil develop-

362 ment. The upper surface of the B<sub>b</sub>-horizon defines the  
363 base of the ATL.

364 Soil pit samples are isotopically well mixed in the  
365 ATL. However, in the B<sub>b</sub>-horizon, nuclide activity  
366 increases with depth (Fig. 8). We interpret the distinct  
367 discontinuity in nuclide activity between the B<sub>b</sub>-horizon  
368 and the ATL in soil pit 1 as either: (1) a hiatus in  
369 deposition, or (2) erosion of material underlying the  
370 current ATL. Consistent with the transect data (Fig.  
371 6), pit 2, located farther from the range front, has  
372 higher <sup>10</sup>Be activity than pit 1. Pit 2 has a smaller,  
373 and for <sup>26</sup>Al, less well-defined step in nuclide activity  
374 at the base of the ATL, implying either less erosion or  
375 a shorter hiatus in deposition.

376  
377 **5.3. Source valley alluvial sediment data**

378 Average <sup>10</sup>Be activities in source valley alluvial  
379 sediment collected along the margins of the Iron and  
380 Granite Mountains are  $1.49 \pm 0.12 \times 10^5$  ( $1\sigma$ ,  $n=3$ )  
381 atoms g<sup>-1</sup> and  $1.40 \pm 0.05 \times 10^5$  ( $1\sigma$ ,  $n=2$ ) atoms g<sup>-1</sup>,  
382 respectively. We did not include GMV-1, because it  
383 was not collected at the range front and, thus, its nuclide  
384 content does not represent sediment generation rates in  
385 the Granite Mountains.

386 **6. Interpretive models of piedmont process**

387 In order to test specific hypotheses and translate our  
388 nuclide-based qualitative understanding of piedmont  
389 process and process history into quantifiable rates and  
390 dates, we used mathematical models to interpret  
391 nuclide measurements. One model interprets source  
392 valley alluvial sediment samples in terms of drainage  
393 basin sediment yield and sediment supply to the  
394 piedmont. A second model uses soil pit nuclide depth  
395 profiles to infer depositional history (Lal and Arnold,  
396 1985; Phillips et al., 1998). A third model tracks  
397 sediment from the time it exits the source basins until  
398 it is deposited or is transported past the last transect  
399 (Fig. 9).

400 In order to make our models tractable, we make  
401 two simplifying assumptions. First, we assume no  
402 preferential dissolution of minerals and, thus, no  
403 quartz enrichment in this arid environment (Small et  
404 al., 1999). Second, because transit times of sediment  
405 across piedmonts are much less than nuclide half lives

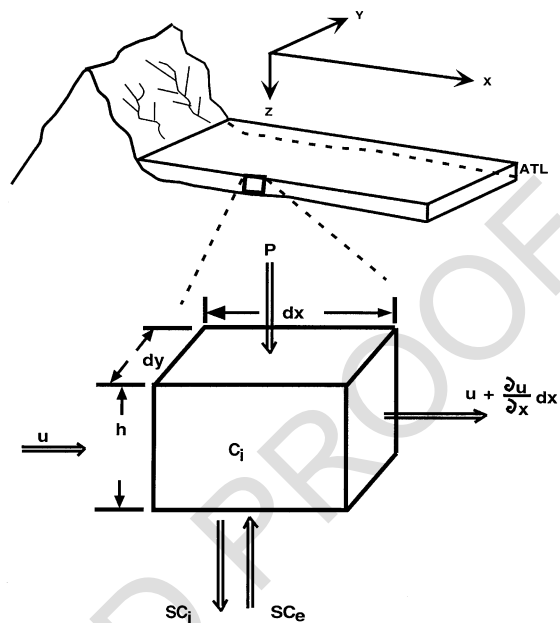


Fig. 9. Schematic of piedmont element model. The piedmont is divided into transport boxes of length, dx, width, dy, and height, h. The double stemmed arrows represent inflows and outflows of nuclides. P is average production during transport, SC<sub>e</sub> is erosion from piedmont beneath ATL, SC<sub>i</sub> is deposition to the piedmont beneath the ATL, u is the flux from up-gradient, and  $u + (\partial u/\partial x)dx$  is the flux out of element box.

and nuclide activity is controlled by surface processes, we disregard radioactive decay.

**6.1. Sediment generation model**

The long-term average sediment generation rate in the mountain drainage basins that supply sediment to the piedmont is modeled from the cosmogenic nuclide data following the work of Brown et al. (1995), Bierman and Steig (1996), and Granger et al. (1996):

$$m = \frac{AP}{C_i(0)}, \tag{1}$$

where m = long-term average basin-wide lowering rate (g cm<sup>-2</sup> a<sup>-1</sup>), A = neutron attenuation factor (165 g cm<sup>-2</sup>), P = spatially weighted nuclide production rate (atoms g<sup>-1</sup> a<sup>-1</sup>), and C<sub>i</sub>(0) = nuclide activity of sediment leaving the basin (atoms g<sup>-1</sup>).

Average basin-wide rock lowering rates, based on <sup>10</sup>Be and <sup>26</sup>Al production rates in Nishiizumi et al.

(1989) are 37 and 39 m Ma<sup>-1</sup>, equivalent to sediment fluxes of 0.13 and 0.097 m<sup>3</sup> a<sup>-1</sup> m<sup>-1</sup>, from the Iron and Granite Mountains, respectively (Table 3). The basin-wide rock lowering rates, based on production rates in Bierman et al. (1996) are 31 and 33 m Ma<sup>-1</sup>, equivalent to sediment fluxes of 0.11 and 0.082 m<sup>3</sup> a<sup>-1</sup> m<sup>-1</sup>, respectively. The Iron and Granite Mountain denudation rates are comparable to those, estimated from analysis of <sup>10</sup>Be and <sup>26</sup>Al in sediment of other landscapes in arid regions. For example, a gneissic sub-basin of Yuma Wash in Arizona is eroding at 30 ± 2 m Ma<sup>-1</sup> (Clapp et al., this issue), and the granite, schist, and gneiss of Nahal Yael drainage basin in the Negev Desert are eroding at 29 ± 6 m Ma<sup>-1</sup> (Clapp et al., 2000). However, the Iron and Granite Mountains are eroding more slowly than semiarid granitic basins in California (60 ± 14 m Ma<sup>-1</sup>) and sandstone basins in New Mexico (101 ± 23 m Ma<sup>-1</sup>) (Granger et al., 1996; Clapp et al., 2001). Erosion rates of granitic landforms are not controlled by precipitation alone as the Iron and Granite Mountains (79 mm a<sup>-1</sup> of precipitation) have erosion rates that are similar to those in the much wetter Luquillo Forest in Puerto Rico (~ 43 m Ma<sup>-1</sup>, >3600 mm a<sup>-1</sup> of precipitation) (Brown et al., 1995).

## 6.2. Soil pit profiles, interpretive model

Soil pit data allow insight into past piedmont processes, specifically the rate at which sediment is added to or lost from the base of the ATL. Stable or eroding surfaces have nuclide profiles that decrease exponentially with depth (Lal and Arnold, 1985) (Fig. 10). In contrast, the nuclide activity in all Iron Mountain soil pit samples collected below the ATL increases with depth (Fig. 8). This increase mandates that the Iron Mountain piedmont must have been a surface of deposition during sometime in the past (Fig. 10).

We can estimate piedmont deposition rates by applying the Lal and Arnold (1985) deposition model to our cosmogenic nuclide soil pit profiles. However, this model assumes constant deposition and does not account for the discontinuity of nuclide activity that we measured at the base of the ATL in both soil pits (Fig. 8). To accommodate the hiatus in deposition that this discontinuity represents, we modify the Lal and Arnold model. Considering the thickness (20 cm at pit 1 and 28 cm at pit 2) and density (1.55 g cm<sup>-3</sup>) of the ATL and its effective shielding of the sediment below, we use an iterative solution to estimate both the deposition rate and the time (represented by the nuclide

t3.1 Table 3  
t3.2 <sup>10</sup>Be and <sup>26</sup>Al erosion rates and associated sediment production rates<sup>a</sup>

Valley location	Basin Area (km <sup>2</sup> )	Production rate (atoms g <sup>-1</sup> a <sup>-1</sup> ) <sup>b</sup>		Production rate (atoms g <sup>-1</sup> a <sup>-1</sup> ) <sup>b</sup>		Erosion rate (m Ma <sup>-1</sup> ) <sup>c</sup>		Sediment generation rate <sup>d</sup> (10 <sup>-2</sup> g cm <sup>-2</sup> a <sup>-1</sup> )		Sediment flux (m <sup>3</sup> a <sup>-1</sup> m <sup>-1</sup> ) <sup>e</sup>	
		<sup>26</sup> Al <sup>f</sup>	<sup>10</sup> Be <sup>g</sup>	<sup>26</sup> Al <sup>h</sup>	<sup>10</sup> Be <sup>i</sup>	<sup>26</sup> Al	<sup>10</sup> Be	<sup>26</sup> Al	<sup>10</sup> Be	<sup>26</sup> Al	<sup>10</sup> Be
t3.3 Iron Mountain	8.1	55.8	9.4	46.5	7.7	35 (29)	39 (33)	0.91 (0.76)	1.03 (0.86)	0.12 (0.10)	0.14 (0.12)
t3.4 Granite Mountain	5.7	56.4	9.5	47.0	7.6	38 (32)	40 (34)	1.04 (0.86)	1.08 (0.84)	0.094 (0.079)	0.099 (0.084)

t3.8 <sup>a</sup> Averages for IMV-1,2,3 and GMV-2,3.

t3.9 <sup>b</sup> Basin-wide, weighted average production rate, differences reflect different basin hypsometry.

t3.10 <sup>c</sup> Rock equivalent (2.7 g cm<sup>-2</sup>), erosion rates based on Bierman et al. (1996) in parentheses.

t3.11 <sup>d</sup> Sediment density = 1.55 g cm<sup>-3</sup>, sediment generation rates based on Bierman et al. (1996) in parentheses.

t3.12 <sup>e</sup> Per unit length of range front (m), sediment flux based on Bierman et al. (1996) in parentheses.

t3.13 <sup>f</sup> Based on high latitude sea-level production rate of 36.8 atoms g<sup>-1</sup> a<sup>-1</sup> (Nishiizumi et al., 1989), scaled to site using Lal et al. (1991), neutrons only.

t3.14 <sup>g</sup> Based on high latitude sea-level production rate of 6.03 atoms g<sup>-1</sup> a<sup>-1</sup> (Nishiizumi et al., 1989), scaled to site using Lal et al., (1991), neutrons only.

t3.15 <sup>h</sup> Based on high latitude sea-level production rate of 30.4 atoms g<sup>-1</sup> a<sup>-1</sup> (Bierman et al., 1996), scaled to site using Lal et al., (1991), neutrons only.

t3.16 <sup>i</sup> Based on high latitude sea-level production rate of 5.17 atoms g<sup>-1</sup> a<sup>-1</sup> (Bierman et al., 1996), scaled to site using Lal et al., (1991), neutrons only.

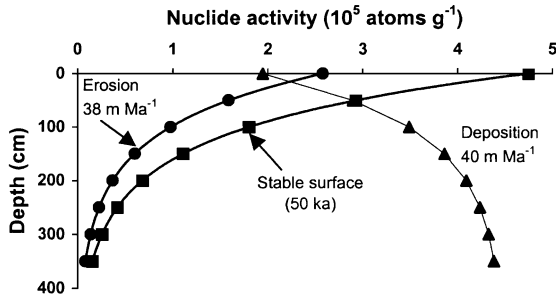


Fig. 10. Stable surfaces (squares) and eroding surfaces (circles) have nuclide activities that decrease at depth. Depositional surfaces (triangles) have nuclide activities that increase with depth. Squares represent a stable surface after 50,000 years of exposure. Circles represent a surface eroding at 38 m Ma<sup>-1</sup>. Triangles represent a 40 m Ma<sup>-1</sup> depositional surface. Data are illustrative for Iron Mountain piedmont latitude and elevation and a soil density of 1.55 g cm<sup>-3</sup>.

474 and physical discontinuity) since deposition ceased  
 475 ( $t_h$ ). Implicit in this calculation is the assumption that  
 476 the ATL existed in its present form and thickness  
 477 during deposition of the underlying material:

$$N = C_i + \frac{1}{D} \int_0^z P_{ATL} e^{\left(\frac{-z\rho}{A}\right)} dz + P_o e^{\left(\frac{-h\rho}{A}\right)} t_h$$

$$= C_i + \frac{P_o A}{D\rho} \left[ 1 - e^{\left(\frac{-z\rho}{A}\right)} \right] + P_o e^{\left(\frac{-h\rho}{A}\right)} t_h, \quad (2)$$

478 where  $N$ =nuclide activity (atoms g<sup>-1</sup>),  $C_i$ =inherited  
 480 nuclide activity at soil pit location (atoms g<sup>-1</sup>),  
 481  $D$ =deposition rate (cm a<sup>-1</sup>),  $h$ =depth of sediment  
 482 sample in soil pit (cm),  $P_{ATL}$ =nuclide production rate  
 483 at base of ATL (atoms g<sup>-1</sup> a<sup>-1</sup>),  $z$ =depth of sediment  
 484 sample below the base of the ATL (cm),  $\rho$ =soil  
 485 density (g cm<sup>-3</sup>),  $P_o$ =nuclide production rate at sur-  
 486 face (atoms g<sup>-1</sup> a<sup>-1</sup>), and  $t_h$ =time of depositional  
 487 hiatus (year).

488 On the Iron Mountain piedmont we have two  
 489 estimates of  $C_i$ . We can use the soil pit data from the  
 490 ATL to estimate  $C_i$ , or we can use the slope of the  
 491 transect data (Fig. 6) to estimate  $C_i$  at the location of  
 492 each soil pit. We report the average of calculated  
 493 deposition rates and hiatus lengths for each estimate  
 494 of  $C_i$ . Using the production rate estimates of Nishiizumi  
 495 et al. (1989), our <sup>10</sup>Be and <sup>26</sup>Al data suggest long-term  
 496 steady-state deposition rates of approximately 21 and  
 497 45 m Ma<sup>-1</sup> for pits 1 and 2, respectively (Fig. 11). The  
 498 average unconformity times for pits 1 and 2 are 8500

and 10,700 years, respectively. Using the production 499  
 rates of Bierman et al. (1996), our <sup>10</sup>Be and <sup>26</sup>Al data 500  
 suggest long-term steady-state deposition rates and 501  
 hiatus times of 17 m Ma<sup>-1</sup> and 10,300 years for pit 1 502  
 and 37.5 m Ma<sup>-1</sup> and 12,500 years for pit 2, respec- 503  
 tively (Fig. 11). 504

These calculations imply a change in piedmont 505  
 behavior apparently coincident with the Pleistocene/ 506  
 Holocene transition about 10,000 years ago. Specific- 507

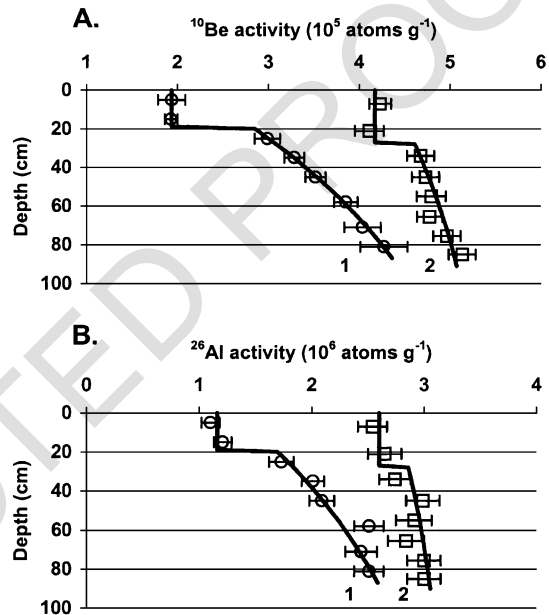


Fig. 11. Predicted deposition rates using (A) <sup>10</sup>Be data, and (B) <sup>26</sup>Al data for soil pit 1 (circles) and soil pit 2 (squares). Black lines represent model fit. <sup>10</sup>Be and <sup>26</sup>Al data are consistent and generate similar deposition rates for respective soil pits. Example is based on using Bierman et al. (1996) production rates and soil pit data to estimate  $C_i$ . Nuclide data for pit 1 suggest uniform deposition (16 m Ma<sup>-1</sup>) from the bottom of the soil pit to 20 cm followed by 14,500 years of stability. Nuclide data for soil pit 2 suggest uniform deposition at 45 m Ma<sup>-1</sup> from the bottom of the soil pit up to 28 cm followed by 7000 years of stability. A discontinuity in nuclide activities at 20 and 28 cm (Pits 1 and 2, respectively) suggests that an active layer above these depths is transporting but not depositing sediment. Different estimates of  $C_i$ , either soil pit data or extrapolation from the slope of transect data (Fig. 6), yield different deposition rates and hiatus times. Using Bierman et al. (1996), nuclide production rates and, averaging the results from the different  $C_i$  estimates, yields average deposition rates and hiatus times of 17 m Ma<sup>-1</sup> and 10,300 years for pit 1, and 38 m Ma<sup>-1</sup> and 12,500 years for pit 2. Using Nishiizumi et al. production rates, the average deposition rate and hiatus time for pit 1 are 21 m Ma<sup>-1</sup> and 8500 years and for pit 2, 45 m Ma<sup>-1</sup> and 10,700 years, respectively.

508 cally, what had been a transport system in which some  
509 mass was lost to the piedmont below, changed to a  
510 regime where sediment moved over, and perhaps  
511 eroded, previously deposited material. These calcula-  
512 tions also imply that sediment was deposited more  
513 slowly closer to the range front. Because surface top-  
514 ography on the piedmont is so subdued, these local  
515 deposition rates probably represent the depositional  
516 histories in a substantial area around each soil pit.  
517 Many more pits would be required to map the history  
518 of deposition over the entire piedmont.

### 520 6.3. Down piedmont sediment transport speeds

521 In order to quantify the average rate at which  
522 grains of sediment move down the Iron and Granite  
523 Mountain piedmonts, we used conceptual models that  
524 consider both nuclide and mass balances. These  
525 models can be developed and employed in a variety  
526 of ways (Small et al., 1999; Nichols, 2000). These  
527 interpretive models rely upon a variety of parameters  
528 some of which we have measured (such as present day  
529 ATL thickness and nuclide activity in sediment enter-  
530 ing the piedmont), some of which we have calculated  
531 (such as mass flux into the piedmont), and some of  
532 which we have taken from the literature (nuclide  
533 production rates). We do not know how well contem-  
534 porary measurements of these parameters (such as  
535 ATL thickness) represent their value in the past, par-  
536 ticularly, in light of changing climate. Therefore, we  
537 modeled a variety of different scenarios to test how  
538 sensitive sediment transport speeds were to model  
539 assumptions and to determine how well our measured  
540 data match predictions made using different model  
541 assumptions.

542 The ATL contains a large volume of sediment. The  
543 length of the Iron Mountain piedmont is 12–15 km and  
544 the average thickness of the ATL is about 25 cm. If the  
545 rate at which sediment is currently delivered from the  
546 Iron Mountain source area ( $0.11 \text{ m}^3 \text{ a}^{-1} \text{ m}^{-1}$ ) is  
547 representative of past rates, then the residence time  
548 for the average grain of sediment in the ATL is about  
549 30,000 years. If some of the material in the ATL were  
550 derived from erosion of the underlying material, resi-  
551 dence time would be shorter. The large volume and  
552 long residence time of sediment in the ATL must buffer  
553 the system against perturbations in sediment delivery  
554 rates, perhaps caused by changing climate.

555 The simplest model for sediment flux across the  
556 piedmont is one in which a column of sediment enters  
557 the ATL from the source area and, as successive  
558 columns are added at the up-piedmont end, this column  
559 moves down the piedmont as a unit. As each column  
560 moves down piedmont in this plug flow scenario, it is  
561 subjected to cosmic ray bombardment and conse-  
562 quently accumulates  $^{10}\text{Be}$  at a rate of about 192 atoms  
563  $\text{cm}^{-2} \text{ a}^{-1}$  (Lal, 1988; Bierman et al., 1996 production  
564 rates). Here, the  $\text{cm}^2$  refers to the surface area of the  
565 column, and the column is assumed to be 25 cm high  
566 ( $h$ ), the mean thickness of the ATL. As the measured  
567 density of the sediment is  $1.55 \text{ g cm}^{-3}$ , this amounts to  
568 an accumulation rate of  $5.0 \text{ }^{10}\text{Be} \text{ atoms g}^{-1} \text{ a}^{-1}$  in the  
569 well-mixed ATL. Sediment moving down the Granite  
570 Mountain piedmont acquires  $^{10}\text{Be}$  at a rate of about  
571  $0.32 \text{ atoms g}^{-1} \text{ cm}^{-1}$  (Fig. 6), implying a speed,  $u$ , of  
572  $\sim 16 \text{ cm a}^{-1}$  and a flux,  $uh$ , of  $390 \text{ cm}^3 \text{ cm}^{-1} \text{ a}^{-1}$ . This  
573 calculated sediment flux is lower by a factor of two than  
574 the flux inferred from nuclide activity in the source  
575 valley alluvial sediment samples, about  $820 \text{ cm}^3 \text{ cm}^{-1}$   
576  $\text{a}^{-1}$  (Table 3). This model implies that the column  
577 would take about 40,000 years to move from the  
578 range front to transect GMT4, 6.2 km from the range-  
579 front.

580 One can consider other scenarios in order to im-  
581 prove the fit of the model to the data. For example, if  
582 erosion of the underlying piedmont is occurring, both  
583 sediment and associated nuclides must enter the ATL.  
584 Assuming the ATL remains 25 cm thick as indicated  
585 by contemporary measurements, the speed of the  
586 column must increase with distance from the range-  
587 front because sediment flux through the ATL is  
588 increasing down piedmont. This flux increase will  
589 have two offsetting effects. On one hand, the increase  
590 in speed will reduce the time available for accumu-  
591 lation of nuclides by production within the column; on  
592 the other hand, the more highly dosed sediment eroded  
593 from the substrate will increase the average concen-  
594 tration in the column.

595 Alternatively, we might assume that the ATL is  
596 increasing in thickness through time as sediment from  
597 the source area is incorporated within it. In this case,  
598 with no erosion of the substrate, the speed of the  
599 column would decrease down slope. This decrease in  
600 speed would lead to a concavity in plots of  $^{10}\text{Be}$  ac-  
601 tivity vs. distance from the range front because, in dis-  
602 tal areas, the more slowly moving column would have

603 more time to accumulate nuclides as it traversed a  
 604 given distance. Such a concavity is evident in the data  
 605 for the Granite Mountain piedmont in Fig. 6 although  
 606 one might argue that it is of marginal statistical  
 607 significance given the uncertainty in the measure-  
 608 ments. There is also a concavity of similar magnitude  
 609 in the data for the Iron Mountain piedmont if one  
 610 ignores the measurements between  $x = -1$  and  $x = 0$ .  
 611 Using the production rate mentioned above and slopes  
 612 of a smooth concave curve through the Granite Moun-  
 613 tain data (Fig. 6), the speed would have to decrease  
 614 from  $\sim 39 \text{ cm a}^{-1}$  in the first kilometer to  $\sim 16 \text{ cm}$   
 615  $\text{a}^{-1}$  between 5 and 6 km from the rangefront.

616 To sort out these possibilities, we developed a  
 617 numerical model of the piedmont. In this model, we  
 618 divided the ATL into boxes of height,  $h$ , length,  $dx$   
 619 (2000 cm), and width,  $dy$  (1 cm) (Fig. 9). The nuclide  
 620 content of a box increases due to production,  $P$ , and  
 621 erosion of the substrate at a rate  $S$ . Thus, during the  
 622 residence time of sediment in the box, taken to be  $dx/$   
 623  $u$ , the concentration of nuclides becomes:

$$C_i = C_{i-1} + (P + SC_e) \frac{dx}{uh}. \quad (3)$$

624 Sediment and nuclides were considered to enter the  
 625 box from the up-piedmont end. This sediment is then  
 626 thoroughly mixed with that already in the box and that  
 627 entering by substrate erosion, thus homogenizing the  
 628 nuclide concentration. The mixing algorithm is:

$$C_i = \frac{(C_{i-1}u + C_i dx)h + C_u S dx}{(u + dx)h + S dx}, \quad (4)$$

630 where  $C_u = C_e \delta + C_i (1 - \delta)$ , and  $\delta = 1$  when  $S > 0$  and 0  
 632 when  $S < 0$ . The effect of the latter relation is to make  
 633 the concentration of nuclides in the sediment entering  
 634 the box through erosion equal to that in the substrate.  
 635 Finally, sediment is passed out of this box at its distal  
 636 end and enters the next box downslope.

637 There are two main differences between the mixing  
 638 model and the column model described above. The  
 639 most important is that mixing is allowed between  
 640 columns and between the underlying piedmont and  
 641 the ATL. This mimics actual processes on the pied-  
 642 mont where there is exchange between sediment in  
 643 transport and sediment that has been residing in the  
 644 ATL for some years. In addition, some lower activity  
 645 sediment could be deposited from the ATL to the

646 piedmont below, or some higher activity sediment  
 647 located in the  $B_b$ -horizon below the ATL could be  
 648 eroded and incorporated into the transport layer. The  
 649 other key difference is that with a numerical model we  
 650 can incorporate changes in  $h$ ,  $S$ , and  $C_e$  with  $x$ .

651 Using measured parameters, we have generated  
 652 models that fit the Iron and Granite transect data well  
 653 (RMS error, 7300 and 10,200 atoms  $\text{g}^{-1}$ , respectively,  
 654 Fig. 12). For both these models, we used the nuclide  
 655 production rates of Bierman et al. (1996), the nuclide-  
 656 based estimates of sediment flux to the piedmont  
 657 (Table 3), the soil pit-based estimates of nuclide  
 658 activity in the top of the underlying  $B_b$ -horizon, the

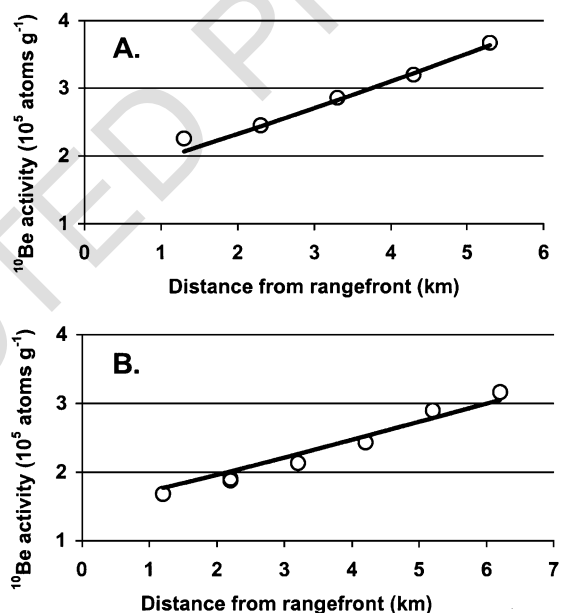


Fig. 12. Predicted (lines) and measured (circles) nuclide activities for Iron (A) and Granite (B) Mountains. Predicted values are from mixing model. RMS errors are low for both Iron Mountain ( $7.3 \times 10^3$  atoms  $\text{g}^{-1}$ ) and Granite Mountain ( $10.2 \times 10^3$  atoms  $\text{g}^{-1}$ ). The following model parameters are the same for both piedmonts:  $P_o = 6.3 \text{ atoms g}^{-1} \text{ a}^{-1}$ ,  $A = 165 \text{ g cm}^{-2}$ ,  $\rho = 1.55 \text{ g cm}^{-3}$ ,  $C_e$  = linear extrapolation between nuclide activity in soil pits of upper  $B_b$  sample corrected for 5000 years of surface exposure below 25 cm ATL. For Iron Mountain:  $h_o$ , the thickness of the ATL at the range front, is 9.0 cm;  $\alpha$ , defined as the down piedmont rate of ATL thickening, is 4.4  $\text{cm km}^{-1}$ ;  $h_{dot}$ , the increase in ATL thickness attributed to incorporation of source valley alluvium sediment, is 0  $\text{cm a}^{-1}$ ;  $q_o$ , the average basin-wide sediment flux, is 1100  $\text{cm}^3 \text{ a}^{-1} \text{ cm}^{-1}$  (Table 3). For Granite Mountain:  $h_o = 16 \text{ cm}$ ,  $\alpha = 3.2 \text{ cm km}^{-1}$ ,  $h_{dot} = 0.0003 \text{ cm a}^{-1}$ ,  $q_o = 820 \text{ cm}^3 \text{ a}^{-1} \text{ cm}^{-1}$  (Table 3).

659 average soil density, and the accepted neutron attenu-  
660 ation factor ( $165 \text{ g cm}^{-2}$ ). Using the parameters listed  
661 above, the only way to fit the measured transect data  
662 (Fig. 6) was to vary the thickness of the ATL over  
663 time and space.

664 In order to fit the Iron Mountain data, the ATL  
665 thickened down piedmont at a rate of  $4.4 \text{ cm km}^{-1}$ .  
666 This resulted in an ATL that thickened from 9.0 cm at  
667 the rangefront to 32 cm at transect 4. Erosion rates of  
668 the underlying piedmont decreased from  $27 \text{ m Ma}^{-1}$   
669 at the rangefront to  $14 \text{ m Ma}^{-1}$  at transect 4. Average  
670 grain speed decreased down piedmont from 122 to 65  
671  $\text{cm a}^{-1}$ . This model resulted in a total transit time  
672 from the rangefront to transect 4 of 6400 years.

673 Although measured nuclide activities increased at a  
674 similar rate down both piedmonts, model results  
675 suggest that the Granite Mountain piedmont behaves  
676 somewhat differently than the Iron Mountain pied-  
677 mont. To fit the Granite Mountain data, we thickened  
678 the ATL at a rate of  $3.2 \text{ cm km}^{-1}$  and allowed de-  
679 position of some sediment from the source area into  
680 the ATL at a rate of  $0.003 \text{ cm a}^{-1}$ . The best fit model  
681 resulted in an ATL that thickened from 13 cm at the  
682 rangefront to 33 cm at transect 4, 6.2 km away.  
683 Erosion rates of the underlying piedmont decreased  
684 from 7 to  $0.6 \text{ m Ma}^{-1}$  over the same distance. Ave-  
685 rage grain speeds are lower than those on the Iron  
686 Mountain piedmont, decreasing down piedmont from  
687 63 to  $24 \text{ cm a}^{-1}$ . This model resulted in a total transit  
688 time from the rangefront to transect 4 of 17,000 years.

689 The mixing model results constrain piedmont be-  
690 havior. Our best fit models for both piedmonts suggest  
691 that sediment is being eroded from below and en-  
692 trained into the ATL, that average grain speed de-  
693 creases down piedmont, and that the geometry of the  
694 ATL changes over time and space. Transit times from  
695 the rangefront to transect 4 range from 6600 to 17,000  
696 years and average grain speed ranges from a few  
697 decimeters to a meter per year. Additional soil pit  
698 nuclide data and developing models that step through  
699 time will probably further increase our understanding  
700 of piedmont behavior.

## 701 7. What we have learned about desert piedmonts

702 In situ produced cosmogenic nuclides trace sedi-  
703 ment movement onto, across, and within desert

piedmonts. Nuclide data allow us to approach funda- 704  
mental questions about piedmont behavior that have 705  
long resisted quantification such as the rates of sedi- 706  
ment transport and deposition across low-gradient 707  
desert surfaces. The combination of amalgamated 708  
transect samples, source-valley alluvial samples, and 709  
soil-pit depth profiles with mass and nuclide balance 710  
models represents a new approach to the application 711  
of cosmogenic nuclides, one that begins to consider 712  
large scale problems in landscape behavior and 713  
history through a quantitative understanding of sedi- 714  
ment movement and sediment budgets over time and 715  
space. 716  
717

### 718 7.1. Piedmonts as dynamic yet organized systems

Nuclide data require that the low gradient granitic 719  
piedmonts we studied are dynamic on a variety of 720  
length and time scales ranging from years to millennia 721  
and meters to kilometers. For example, nuclide anal- 722  
yses and field observations suggest that lateral and 723  
shallow vertical sediment mixing processes are impor- 724  
tant and rapid on granitic desert piedmonts. Mixing is 725  
done by animal burrowing and by the random avul- 726  
sion, incision, and filling of the shallow ephemeral 727  
channels that criss-cross the piedmont surface (Nichols 728  
and Bierman, in press). Low-relief (dm-scale) geo- 729  
morphic units (channels and terraces) have indistin- 730  
guishable nuclide activities (Fig. 4), suggesting that 731  
braided ephemeral channels migrate across the pied- 732  
mont surface on  $10^2$  to  $10^3$  years time scales, reshaping 733  
surface microtopography. Depth profiles (Fig. 8) and 734  
nuclide analysis of sediment brought to the surface by 735  
burrowing animals reveal that the uppermost 20 to 30 736  
cm of piedmont sediment is well and continually 737  
mixed over a time scale comparable to that for lateral 738  
mixing. 739

740 Within this well-mixed system there is order.  
741 Nuclide activity increases uniformly down both pied-  
742 monts (Fig. 6). The regular increase in average nuclide  
743 activity as a function of distance from the rangefront  
744 indicates that the locally and temporally chaotic pied-  
745 mont sediment transport system functions in a predict-  
746 able, uniform fashion over length and time scales that  
747 our amalgamated samples represent (km) and can  
748 resolve (ka). Individual grains are brought down pied-  
749 mont in an episodic series of transport events, each  
750 presumably of varying length, between which the

751 grains are stored and dosed by cosmic radiation. The  
 752 regular increase in average nuclide activity down pied-  
 753 mont reflects the slow, episodic, but ongoing transport  
 754 of grains from mountain sources to the piedmont and  
 755 ultimately, in the case of some of the finer grains, to  
 756 playa sinks.

### 758 7.2. Piedmont history

759 Both geologic and isotopic evidence, the marked  
 760 discontinuity in soil color and nuclide activity at the  
 761 base of today's well-mixed active layer, require that  
 762 the behavior and sediment budget of the Iron Mountain  
 763 piedmont changed during the Late Pleistocene or Early  
 764 Holocene epoch. Soil pit data (Section 6.2), specifi-  
 765 cally the general increase in nuclide activity with depth  
 766 below the ATL, suggest steady deposition occurred on  
 767 the piedmont prior to about 10,000 years ago at rates  
 768 between 17 and 45 m Ma<sup>-1</sup>. In contrast, there is no  
 769 stratigraphic or isotopic evidence of Holocene depo-  
 770 sition from the ATL into the substrate below. As long  
 771 as there has been rapid channel migration that cur-  
 772 rently characterizes water and sediment transport on  
 773 these granitic piedmonts, there will be a well-mixed  
 774 layer of surface sediment. The thickness of such an  
 775 ATL through time cannot be constrained by field  
 776 measurements and likely varies as a result of changes  
 777 in sediment supply, climate, and piedmont hydrology;  
 778 however, modeling can suggest reasonable values of  
 779 ATL thickness in the past.

780 The end of the Pleistocene was a time when mois-  
 781 ture effectiveness and vegetative cover decreased in  
 782 the Mojave (Spaulding et al., 1983). Bull and Schick  
 783 (1979) and Bull (1991) argued that such a climate  
 784 change would result in a pulse of hillslope erosion and,  
 785 thus, piedmont aggradation as drainage basin soils, no  
 786 longer well anchored by vegetation and subjected to  
 787 increasingly variable precipitation, were stripped from  
 788 hillslopes. Our data are consistent with a piedmont  
 789 process change at the Pleistocene/Holocene transition  
 790 that could have been occasioned by a change in sedi-  
 791 ment yield and basin hydrology. However, even if  
 792 sediment yield increased as postulated by Bull, soil pit  
 793 nuclide data clearly show that such an increase did not  
 794 cause deposition from the ATL to the piedmont below.  
 795 It is possible that ATL thickness, which is controlled  
 796 by the depth of migrating ephemeral channels (Nichols  
 797 and Bierman, in press), increased in response to

changing runoff patterns and, thus, accommodated  
 sediment stripped from the basins.<sup>1</sup>

### 7.3. Sediment transport rates

Sediment transport rates across desert piedmonts,  
 expressed as average grain speeds, have been unknown  
 until now. Although there remains some uncertainty in  
 nuclide and sediment production rates and in the flux of  
 sediment delivered from the source basins, average  
 grain speeds on the Iron Mountain piedmont range  
 from a few decimeters to a meter per year. Such low  
 speeds imply that human disturbance or sediment  
 contamination would have long-lasting effects on des-  
 ert piedmonts. Average sediment grains that are not  
 deposited into long-term storage still remain on the  
 piedmont for up to tens of thousands of years as they  
 move from mountains to the playa.

### 7.4. Application to the "pediment problem"

The piedmonts that we studied are low relief, planar  
 surfaces where sand and fine gravel are transported  
 from the abutting granitic highlands to distant lowland  
 basins. Classifying these piedmont surfaces is not  
 straightforward. They are pediment-like in their planar  
 morphology and in the existence of an active transport  
 layer over an indurated, and perhaps beveled, sub-  
 strate. They are fan-like in that deposition dominated  
 the piedmont surface over the later Pleistocene.

Whatever term is used to describe the Granite and  
 Iron Mountain piedmonts, our data are consistent with  
 a geomorphic system dominated by rapidly migrating  
 channels, spatially homogeneous braided drainage,  
 planar morphology, and a uniform substrate lithology.  
 Homogeneity of a piedmont drainage network is rep-

<sup>1</sup> One of us (RLH) interprets the available data differently. Although there must be an ATL whenever fluvial deposition is occurring on such a piedmont, Hooke suspects that deposition on this piedmont effectively ceased prior to the last major pluvial period in the Mojave. During this pluvial, runoff may have been confined, by vegetation, to more permanent and more stable channels. During this hiatus, lasting 10 to 20 ka, weathering resulted in the observed red B<sub>b</sub> horizon. Upon return to arid conditions at the end of the Pleistocene, according to this interpretation, channels began to migrate more freely across the piedmont surface and the present ATL began to form from a mixture of new material derived from the source area and old material from erosion of the B<sub>b</sub>.

resented numerically by a “random walk” of channels over uniform lithology (Rachocki, 1981). Results of such a model show that where alluvial fans coalesce, drainage becomes an interconnected network of braided channels, the discharge of channels becomes uniform, and the “. . .coalesced surface forms an alluvial piedmont plain.” Individual channel morphometry on the Iron Mountain piedmont does not vary significantly over the piedmont’s width or length (Nichols and Bierman, in press) consistent with Rachocki’s findings.

Weak channel banks and rapid changes in discharge are typical of migrating channels in sediment-laden networks (Ritter, 1978) and allow for rapid migration of channels over either more resistant bedrock or more indurated sediment. Rapid channel migration, such as we have demonstrated isotopically at Iron Mountain, could effectively bevel high spots on piedmonts and maintain a planar morphology without forming entrenched channels. This lateral erosion process is consistent with the ideas of Gilbert (1877) and Paige (1912), who were the first to speculate that such a process contributes to pedimentation.

7.5. *Implications for the application of cosmogenic nuclides to geomorphic problems*

This study integrates several different applications of in situ produced cosmogenic nuclides in an attempt to understand better a geomorphic system. The amalgamated transect technique, developed and presented in this paper, averages out point to point differences and elucidates large-scale trends in nuclide activity and, thus, landscape behavior. While sample collection is time intensive, the number of samples generated is modest and the surface area over which the results are relevant is quite large. Simple models allow for determination of a sediment budget for the Iron and Granite Mountain piedmont systems and, thus, calculation of average grain speeds across piedmont surfaces. Depth profiles of nuclide activity in soils allow us to infer past behavior of piedmont systems as well as allowing estimation of sediment deposition rates over time (Lal and Arnold, 1985; Brown et al., 1995; Phillips et al., 1998); however, depth profiles are sample intensive and representative of only modestly sized areas near the soil pit. All of the field and analytical approaches that we have used could be applied in any number of different geomorphic settings.

Measuring and interpreting cosmogenic nuclide activities allow us to quantify sediment transport rates and piedmont processes on a  $10^3$  to  $10^5$  years time scale, much shorter than the time of formation of many desert piedmonts (Cooke and Warren, 1973; Oberlander, 1974), but much longer than the duration of contemporary process studies (Abrahams et al., 1984; Lekach and Schick, 1999; Yair, 1999). Thus, our results describe piedmont behavior and piedmont modification and begin to approach the question of piedmont genesis. Such an understanding will only come when a variety of data including underlying structure, lithology, and the geometry of sediment cover are integrated fully with modern process studies, cosmogenic rate data, and mass balance models.

Although this investigation focuses on one area, the similar increase of nuclide activity down both the Iron and Granite Mountain piedmonts suggests that our findings can probably be generalized to other granitic piedmonts in similar tectonic and climatic settings. Applying this technique to piedmonts with different lithologies, slopes, tectonic settings, climates, and morphologies will provide a better understanding of the rate, history, and distribution of desert piedmont processes throughout the world.

## Acknowledgements

We thank D. Santos and C. Massey for field assistance, D. Howell for statistical assistance, B. Copans and S. Neis for laboratory assistance, and D. Dethier and S. Brown (Williams College) for assistance with carbonate analyses. E. Steig provided helpful comments on an earlier version of this manuscript. Funding for this project was provided by U.S. Army Research Office grants DAAG559710180 and DAAH049610036, and in part by the U.S. Department of Energy contract No. W-7405-Eng-48, and National Science Foundation grants EAR 9628559 and MRI EAR 9724190.

## References

- Abrahams, A.D., Parsons, A.J., Cooke, R.U., Reeves, R.W., 1984. Stone movement on hillslopes in the Mojave Desert, California: a 16-year record. *Earth Surf. Processes and Landforms* 9, 365–370.

- 922 Bierman, P.R., Steig, E.J., 1996. Estimating rates of denudation  
923 using cosmogenic isotope abundances in sediment. *Earth Surf.*  
924 *Processes and Landforms* 21, 125–139.
- 925 Bierman, P., Larsen, P., Clapp, E., Clark, D., 1996. Refining estimates  
926 of  $^{10}\text{Be}$  and  $^{26}\text{Al}$  production rates. *Radiocarbon* 38, 149.
- 927 Birkeland, P.W., 1984. *Soils and Geomorphology*. Oxford Univ.  
928 Press, New York, 372 pp.
- 929 Brown, E.T., Stallard, R.F., Larsen, M.C., Raisbeck, G.M., Yiou, F.,  
930 1995. Denudation rates determined from the accumulation of in  
931 situ-produced  $^{10}\text{Be}$  in the Luquillo Experimental Forest, Puerto  
932 Rico. *Earth Planet. Sci. Lett.* 129, 193–202.
- 933 Bull, W.B., 1977. The alluvial-fan environment. *Prog. Phys. Geogr.*  
934 1, 222–270.
- 935 Bull, W.B., 1991. *Geomorphic Responses to Climatic Change*. Ox-  
936 ford Univ. Press, New York, 326 pp.
- 937 Bull, W.B., Schick, A.P., 1979. Impact of climatic change on an  
938 arid watershed: Nahal Yael, southern Israel. *Quat. Res.* 11,  
939 153–171.
- 940 Clapp, E.M., Bierman, P.R., Schick, A.P., Lekach, J., Enzel, Y.,  
941 Caffee, M., 2000. Sediment yield exceeds sediment production  
942 in arid region drainage basins. *Geology* 28, 995–998.
- 943 Clapp, E.M., Bierman, P.R., Nichols, K.K., Pavich, M., Caffee, M.,  
944 2001. Rates of sediment supply to arroyos from upland erosion  
945 determined using in situ-produced cosmogenic  $^{10}\text{Be}$  and  $^{26}\text{Al}$ .  
946 *Quat. Res.* 55, 235–245.
- 947 Clapp, E.M., Bierman, P.R., Caffee, M., this issue. Using  $^{10}\text{Be}$  and  
948  $^{26}\text{Al}$  to determine sediment generation rates and identify sediment  
949 source areas in an arid region drainage basin. *Geomorphology*.
- 950 Clark, D.H., Bierman, P.R., Larsen, P., 1995. Improving in situ  
951 cosmogenic chronometers. *Quat. Res.* 44, 367–377.
- 952 Cooke, R.U., Warren, A., 1973. *Geomorphology in Deserts*. Univ.  
953 California Press, Berkeley, 394 pp.
- 954 Denny, C.S., 1967. Fans and pediments. *Am. J. Sci.* 265, 81–105.
- 955 Desilets, D., Zreda, M., 2000. Scaling production rates of terrestrial  
956 cosmogenic nuclides for altitude and geomagnetic effects. *Geol.*  
957 *Soc. Am. Abstr. Programs* 31, 400.
- 958 Dohrenwend, J.C., 1987. Basin and range. In: Graf, W.L. (Ed.),  
959 *Geomorphic Systems of North America. Decade of North Amer-*  
960 *ica Geology. Geol. Soc. Am., Boulder, Colorado, Centen. Spec.,*  
961 *vol. 2, pp. 303–342.*
- 962 Dunai, T., 2000. Scaling factors for production rates of in situ  
963 produced cosmogenic nuclides: a critical reevaluation. *Earth*  
964 *Planet. Sci. Lett.* 176, 157–169.
- 965 Gilbert, G.K., 1877. *Geology of the Henry Mountains (Utah)*. U.S.  
966 *Geographical and Geological Survey of the Rocky Mountain*  
967 *Region*. Washington, DC.
- 968 Granger, D.E., Kirchner, J.W., Finkel, R., 1996. Spatially averaged  
969 long-term erosion rates measured from in situ produced cosmo-  
970 genic nuclides in alluvial sediment. *J. Geol.* 104, 249–257.
- 971 Greenbaum, N., Salmon, O., Gerson, R., Schick, A.P., 1999. Slope  
972 runoff in a hyperarid region. In: Lekach, J., Hassan, M.A. (Eds.),  
973 *Drainage Basin Dynamics and Morphology: Conference Excur-*  
974 *sion-Negev Desert (Excursion Guide)*. Hebrew Univ., Jerusalem,  
975 pp. 104–110.
- 976 Hooke, R.L., 1968. Steady-state relationships on arid-region alluvial  
977 fans in closed basins. *Am. J. Sci.* 266, 609–629.
- 978 Kohl, C.P., Nishiizumi, K., 1992. Chemical isolation of quartz for  
measurement of in situ-produced cosmogenic nuclides. *Geo-*  
chim. *Cosmochim. Acta* 56, 3583–3587. 979  
980
- Lal, D., 1988. In situ-produced cosmogenic isotopes in terrestrial  
981 rocks. *Ann. Rev. Earth Planet. Sci.* 16, 355–388. 982
- Lal, D., 1991. Cosmic ray labeling of erosion surfaces: in situ nuclide  
983 production rates and erosion models. *Earth Planet. Sci. Lett.* 104,  
984 424–439. 985
- Lal, D., Arnold, J.R., 1985. Tracing quartz through the environment.  
986 *Proc. Indian Acad. Sci.* 94, 1–5. 987
- Laronne, J.B., Reid, I., 1993. Very high rates of bedload sediment  
988 transport by ephemeral desert rivers. *Nature* 366, 148–150. 989
- Laronne, J.B., Reid, I., Yitshak, Y., Frostick, L.E., 1994. The non-  
990 layering of gravel streambeds under ephemeral flood regimes. *J.*  
991 *Hydrol.* 159, 353–363. 992
- Lekach, J., Schick, A.P., 1999. Sediment transport and sediment  
993 yield. In: Lekach, J., Hassan, M.A. (Eds.), *Drainage Basin Dy-*  
994 *namics and Morphology: Conference Excursion-Negev Desert*  
995 *(Excursion Guide)*. Hebrew Univ., Jerusalem, pp. 89–97. 996
- Lekach, J., Amit, R., Grodek, T., Schick, A.P., 1998. Fluvio-pedo-  
997 genic processes in an ephemeral stream channel. Nahal Yael,  
998 Southern Negev, Israel. *Geomorphology* 23, 353–369. 999
- Machette, M., 1986. Calcium and magnesium carbonates. In: Sing-  
1000 er, M.J., Janitzky, P. (Eds.), *Field and Laboratory Procedures*  
1001 *Used in a Soil Chronosequence Study*. U.S. Geol. Surv., Reston,  
1002 VI, pp. 30–33. 1003
- Mayer, L., Bull, W.B., 1981. Impact of Pleistocene–Holocene cli-  
1004 matic change on particle size distribution of fan deposits in  
1005 southwestern Arizona. *Geol. Soc. Am. Abstr. Programs* 13, 95. 1006
- McFadden, L.D., Ritter, J.B., Wells, S.G., 1989. Use of multipara-  
1007 meter relative-age methods for age estimation and correlation of  
1008 alluvial fansurfaces on a desert piedmont, eastern Mojave Des-  
1009 ert, California. *Quat. Res.* 32, 276–290. 1010
- Nichols, K.K., 2000. A multiscale approach to understanding desert  
1011 piedmonts using cosmogenic isotopes and centimeter-scale sur-  
1012 veying. MSc Thesis, Univ. Vermont, Burlington, VT, 264 pp. 1013
- Nichols, K.K., Bierman, P.R., in press. Fifty-four years of ephemer-  
1014 al channel response to two years of intense World War II  
1015 military activity, Camp Iron Mountain, Mojave Desert, Califor-  
1016 nia. In: Ehlen, J., Harmon, R.S. (Eds.), *The Environmental Leg-*  
1017 *acy of Military Operations*. *Rev. Eng. Geol.*, 14. 1018
- Nishiizumi, K., Winterer, E.L., Kohl, C.P., Klein, J., Middleton, R.,  
1019 Lal, D., Arnold, J.R., 1989. Cosmic ray production rates of  $^{10}\text{Be}$   
1020 and  $^{26}\text{Al}$  in quartz from glacially polished rocks. *J. Geophys. Res.*  
1021 94, 17907–17915. 1022
- NOAA, 1982. Monthly normals of temperature, precipitation, and  
1023 heating and cooling degree days 1951–1980, California, U.S.  
1024 National Oceanic and Atmospheric Administration (NOAA),  
1025 Asheville, NC. 1026
- Oberlander, T.M., 1974. Landscape inheritance and the pediment  
1027 problem in the Mojave Desert of southern California. *Am. J.*  
1028 *Sci.* 274, 849–875. 1029
- Paige, S., 1912. Rock-cut surfaces in desert ranges. *J. Geol.* 20,  
1030 442–450. 1031
- Phillips, W.M., McDonald, E.V., Reneau, S.L., Poets, J., 1998.  
1032 Dating soils and alluvium with cosmogenic  $^{21}\text{Ne}$  depth profiles:  
1033 case studies from the Pajarito Plateau, New Mexico, USA. *Earth*  
1034 *Planet. Sci. Lett.* 160, 209–223. 1035

- 1036 Rachocki, A., 1981. Alluvial Fans an Attempt at an Empirical Ap-  
1037 proach. Wiley, New York, 161 pp.
- 1038 Reid, I., Laronne, J.B., 1995. Bed load sediment transport in an  
1039 ephemeral stream and a comparison with seasonal and perennial  
1040 counterparts. *Water Resour. Res.* 31, 773–781.
- 1041 Ritter, D.F., 1978. *Process Geomorphology*. W.M.C. Brown, Debu-  
1042 que, IA, 603 pp.
- 1043 Small, E.E., Anderson, R.S., Hancock, G.S., 1999. Estimates of the  
1044 rate of regolith production using  $^{10}\text{Be}$  and  $^{26}\text{Al}$  from an alpine  
1045 hillslope. *Geomorphology* 27, 131–150.
- 1046 Spaulding, W.G., Graumlich, L.J., 1986. The last pluvial climatic  
1047 episodes in the deserts of southwestern North America. *Nature*  
1048 320, 441–444.
- Spaulding, W.G., Leopold, E.B., van Devender, T.R., 1983. Late 1049  
Wisconsin paleoecology of the American southwest. In: Wright, 1050  
H.E. (Ed.), *Late-Quaternary Environments of the United States*. 1051  
Porter, S.C. (Ed.), *The Late Pleistocene*, vol. 1, Univ. Minnesota 1052  
Press, Minneapolis, pp. 259–293. 1053
- Wells, S.G., McFadden, L.D., Dohrenwend, J.C., 1987. Influence of 1054  
Late Quaternary climatic changes on geomorphic and pedogenic 1055  
processes on a desert piedmont, eastern Mojave Desert, Califor- 1056  
nia. *Quat. Res.* 27, 130–146. 1057
- Yair, A., 1999. Sede Boquer research site. In: Lekach, J., Hassan, 1058  
M.A. (Eds.), *Drainage Basin Dynamics and Morphology: Con- 1059  
ference Excursion-Negev Desert (Excursion Guide)*. Hebrew 1060  
Univ., Jerusalem, pp. 18–51. 1061